Earth and Planetary Science Letters 434 (2016) 1–9

Contents lists available at ScienceDirect

Earth and Planetary Science Letters

www.elsevier.com/locate/epsl

Constraining the oceanic barium cycle with stable barium isotopes

Zhimian Cao [a,b,*], Christopher Siebert [a], Ed C. Hathorne [a], Minhan Dai [b], Martin Frank [a]

[a] GEOMAR Helmholtz Center for Ocean Research Kiel, Wischhofstrasse 1-3, Kiel 24148, Germany
[b] State Key Laboratory of Marine Environmental Science, Xiamen University, Xiang'an District, Xiamen 361102, China

ARTICLE INFO

Article history:
Received 13 August 2015
Received in revised form 8 November 2015
Accepted 12 November 2015
Available online 28 November 2015
Editor: D. Vance

Keywords:
seawater Ba isotopes
nutrient-like fractionation
water mass mixing
proxy
oceanic Ba dynamics

ABSTRACT

The distribution of barium (Ba) concentrations in seawater resembles that of nutrients and Ba has been widely used as a proxy of paleoproductivity. However, the exact mechanisms controlling the nutrient-like behavior, and thus the fundamentals of Ba chemistry in the ocean, have not been fully resolved. Here we present a set of full water column dissolved Ba (DBa) isotope ($\delta^{137}Ba_{DBa}$) profiles from the South China Sea and the East China Sea that receives large freshwater inputs from the Changjiang (Yangtze River). We find pronounced and systematic horizontal and depth dependent $\delta^{137}Ba_{DBa}$ gradients. Beyond the river influence characterized by generally light signatures (0.0 to +0.3‰), the $\delta^{137}Ba_{DBa}$ values in the upper water column are significantly higher (+0.9‰) than those in the deep waters (+0.5‰). Moreover, $\delta^{137}Ba_{DBa}$ signatures are essentially constant in the entire upper 100 m, in which dissolved silicon isotopes are fractionated during diatom growth resulting in the heaviest isotopic compositions in the very surface waters. Combined with the decoupling of DBa concentrations and $\delta^{137}Ba_{DBa}$ from the concentrations of nitrate and phosphate this implies that the apparent nutrient-like fractionation of Ba isotopes in seawater is primarily induced by preferential adsorption of the lighter isotopes onto biogenic particles rather than by biological utilization. The subsurface $\delta^{137}Ba_{DBa}$ distribution is dominated by water mass mixing. The application of stable Ba isotopes as a proxy for nutrient cycling should therefore be considered with caution and both biological and physical processes need to be considered. Clearly, however, Ba isotopes show great potential as a new tracer for land–sea interactions and ocean mixing processes.

1. Introduction

The nutrient-like distribution of dissolved barium (DBa) in seawater, resembling that of silicate ($Si(OH)_4$) with low surface and elevated deep water concentrations (Bacon and Edmond, 1972; Lea and Boyle, 1989; Jeandel et al., 1996; Jacquet et al., 2005; Roeske et al., 2012), is commonly attributed to the biologically mediated incorporation of DBa in or adsorption onto biogenic particles in the upper ocean and regeneration via particle dissolution and/or degradation at depth (Dehairs et al., 1980; Paytan and Griffith, 2007). Importantly, within this cycle, a maximum of excess (or biogenic) particulate Ba (Ba_{xs}), most likely resulting from barite ($BaSO_4$) precipitation in oversaturated microenvironments generated by degradation of sinking organic aggregates, is frequently observed in the mesopelagic zone between 100 and 600 m water depth (Dehairs et al., 1997; Jacquet et al., 2005). Therefore, Ba_{xs} or barite fluxes to the deep ocean and their accumulation rates in sediments have been widely applied to reconstruct export productivity (Paytan et al., 1996; Nürnberg et al., 1997; Paytan and Griffith, 2007). However, the exact mechanisms controlling the behavior of DBa and the mesopelagic Ba_{xs} maximum are not fully understood (Ganeshram et al., 2003; Jacquet et al., 2005). Moreover, the poor preservation of barite in sediments under suboxic conditions complicates the interpretation of its paleoceanographic record (McManus et al., 1998).

Recently, the first measurements of mass-dependent stable Ba isotope fractionation have been reported (von Allmen et al., 2010; Böttcher et al., 2012; Miyazaki et al., 2014; Horner et al., 2015; Nan et al., 2015), which provide a new avenue to better understand the biogeochemistry of Ba in the ocean and thus to extend and improve its applicability as a paleoproxy. This pioneering work showed that measurable differences of Ba isotopic compositions (−0.5 to +0.1‰) exist between natural Ba minerals of various origins. Lighter Ba isotopes are enriched in Ba precipitates produced in the laboratory relative to the corresponding aqueous solutions, probably due to reaction kinetics or sur-

* Corresponding author at: GEOMAR Helmholtz Center for Ocean Research Kiel, Wischhofstrasse 1-3, Kiel 24148, Germany. Tel.: +49 431 6002254; fax: +49 431 6002925.
E-mail address: zcao@geomar.de (Z. Cao).

http://dx.doi.org/10.1016/j.epsl.2015.11.017
0012-821X/

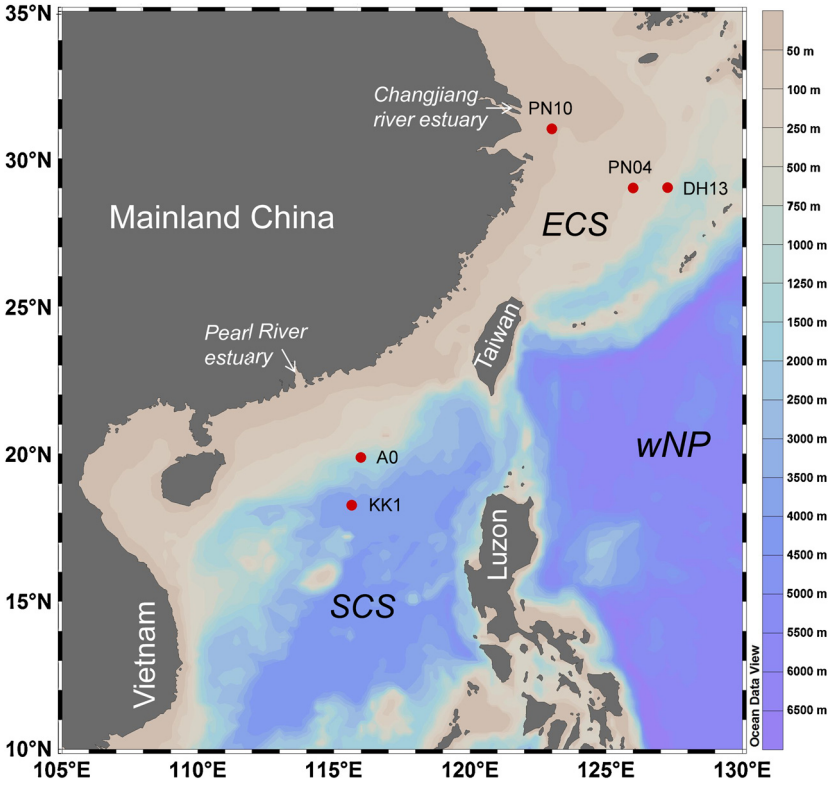

Fig. 1. Bathymetric map of the East China Sea (ECS) and the South China Sea (SCS) showing the locations of sampling stations. The bottom depths of stations PN10, PN04, DH13, A0, and KK1 are ~50 m, ~120 m, ~600 m, ~1450 m, and ~3800 m, respectively. The Changjiang (Yangtze River) and the Pearl River are two of the world's largest river systems feeding the ECS and the northern SCS, respectively. wNP: western North Pacific. The map was created with ODV (Schlitzer, 2015). (For interpretation of the colors in this figure, the reader is referred to the web version of this article.)

face entrapment of the lighter isotopes (Immenhauser et al., 2010; von Allmen et al., 2010). A seawater profile in the South Atlantic showed that Ba isotopic compositions generally decrease with water depth (Horner et al., 2015). Consequently, given the direct involvement of Ba in various biological and chemical processes, fractionation of stable Ba isotopes in seawater has the potential to provide information on nutrient cycling, productivity and water mass mixing.

With the goal to establish a framework for the use of oceanic Ba isotope fractionation as a proxy, we analyzed dissolved Ba isotopic compositions ($\delta^{137}Ba_{DBa}$) from different marine regimes in four seawater profiles collected in the East China Sea and the South China Sea, extending from the inner shelf influenced by a large river plume (Zhai and Dai, 2009) to the deep South China Sea basin, which is analogous to an open ocean setting (Cao and Dai, 2011). δ^{137}Ba signatures of Ba_{xs} in suspended particles ($\delta^{137}Ba_{Baxs}$) were also determined for the upper 150 m of the water column at one station in the South China Sea (Fig. 1; Tables 1 and 2). In addition, $\delta^{137}Ba_{DBa}$ was measured in samples collected from eight rivers around the world to assess the isotopic composition of the major Ba source to the ocean (Table 3). Given the close relationship between DBa and $Si(OH)_4$ concentrations generally observed in the world's oceans (Bacon and Edmond, 1972; Lea and Boyle, 1989; Jeandel et al., 1996; Jacquet et al., 2005; Roeske et al., 2012), we compared our seawater $\delta^{137}Ba_{DBa}$ data with the corresponding dissolved Si isotope signatures ($\delta^{30}Si_{Si(OH)_4}$; Cao et al., 2012, 2015). We also compared our Ba results with the distribution of other major nutrient (nitrate (NO_3) and phosphate (PO_4)) concentrations in order to further constrain the biological effects on seawater Ba isotopic compositions.

2. Materials and methods

2.1. Sampling

In August 2009, seawater samples for DBa concentration and $\delta^{137}Ba_{DBa}$ analyses were collected at stations PN10 (located on the inner shelf), PN04 (mid-shelf), and DH13 (continental slope) of the East China Sea (Cao et al., 2015). In January 2010, this sample set was extended by station KK1 located in the north basin of the South China Sea (Fig. 1). 60–250 mL of seawater was collected with Niskin bottles attached to a Rosette sampler and filtered through 0.45 μm nitrocellulose acetate filters into acid precleaned polyethylene bottles immediately after sampling. Samples were subsequently acidified to pH~2 with distilled concentrated HCl (0.1% v/v) and stored at room temperature in the dark until analysis in the laboratory. In addition, filtered and acidified water samples were collected from various global rivers (Table 3).

In August 2009, suspended particle samples for Ba_{xs} concentration and isotopic composition ($\delta^{137}Ba_{Baxs}$) analyses were obtained at station A0 in the South China Sea (Fig. 1) by filtering ~6 L of seawater through 0.4 μm polycarbonate membranes. The membranes were dried at 50 °C overnight and stored in polycarbonate dishes until analysis in the laboratory.

2.2. Ba isotope analyses

Here we summarize the method for Ba isotope measurements using a double spike technique. Further details are provided in the Supplementary Material.

Table 1
Salinity, dissolved barium (DBa) concentration and their stable barium isotopic composition ($\delta^{137}Ba_{DBa}$) data collected in the East China Sea (ECS) in August 2009 and in the South China Sea (SCS) in January 2010.

Cruise	Station	Depth[a] (m)	Salinity[a]	DBa (nmol kg^{-1})	$\delta^{137}Ba_{DBa}$ (‰)	2SD[b] (‰)	n[c]
ECS	PN10	1.3	25.89	175.8	0.45	0.07	3
August 2009	31.0°N 123.0°E	1.3	duplicate		0.47	0.11	4
		4.5	27.17	161.5	0.42	0.07	4
		14.9	32.22	70.0	0.54	0.09	2
		14.9	duplicate		0.45	0.12	3
		25.1	34.00	51.2			
		35.5	34.11	50.0			
		46.9	34.13	50.7	0.66	0.09	3
		46.9	duplicate		0.59	0.09	4
	PN04	2.0	33.74	40.6	0.98	0.08	2
	29.0°N 126.0°E	24.4	33.83	40.4	0.87	0.13	3
		49.4	33.85	38.9			
		73.8	34.10	38.5			
		99.8	34.50	39.7			
		117.7	34.50	39.2	0.90	0.03	2
	DH13	3.2	33.73	36.6	0.89	0.04	2
	29.0°N 127.3°E	3.2	duplicate		0.76	0.08	3
		25.1	33.82	35.7	0.93	0.08	3
		49.6	33.99	37.2			
		73.8	34.18	39.8			
		98.6	34.39	39.8	0.99	0.11	2
		123.7	34.61	40.8	0.81	0.09	3
		123.7	duplicate		0.74	0.10	4
		148.6	34.49	44.4			
		198.5	34.45	45.7	0.62	0.07	3
		297.3	34.37	52.0			
		553.7	34.33	72.9	0.45	0.04	3
		553.7	duplicate		0.56	0.03	3
SCS	KK1	5.2	33.88	40.2	0.90	0.10	3
January 2010	18.3°N 115.7°E	19.6	33.88	38.4	1.03	0.12	3
		50.1	34.10	41.4	0.91	0.07	3
		50.1	duplicate		1.04	0.04	2
		79.8	34.49	40.4			
		98.3	34.57	40.6	0.86	0.05	3
		98.3	duplicate		0.86	0.17	2
		149.9	34.59	45.6			
		198.5	34.53	49.2	0.88	0.06	3
		198.5	duplicate		0.77	0.15	3
		301.0	34.44	55.9			
		499.2	34.41	75.5	0.67	0.05	3
		499.2	duplicate		0.60	0.16	3
		798.3	34.48	98.8	0.56	0.09	4
		1000.9	34.53	112.7	0.57	0.08	3
		1000.9	duplicate		0.52	0.09	3
		1500.5	34.59	133.8	0.54	0.12	3
		2499.1	34.61	136.6	0.51	0.06	3
		3644.6	34.61	134.9	0.58	0.02	3
		3644.6	duplicate		0.54	0.11	3

[a] Depth and salinity data collected in the ECS are from Cao et al. (2015).
[b] SD is the standard deviation estimated from the double spike bracketing measurements of a single sample solution.
[c] n is the number of double spike bracketing measurements of a single sample solution.

Table 2
Excess particulate barium (Ba_{xs}) concentration and their stable barium isotopic composition ($\delta^{137}Ba_{Baxs}$) data collected in the upper 150 m of the water column at station A0 in the South China Sea (SCS).

Cruise	Station	Depth (m)	Ba_{xs} (nmol kg^{-1})	$\delta^{137}Ba_{Baxs}$ (‰)	2SD[a] (‰)	n[b]
SCS	A0	5.2	0.6	0.24	0.08	2
August 2009	19.9°N 116.0°E	52.6	5.3	0.23	0.10	3
			duplicate	0.20	0.04	4
		75.0	1.3	0.22	0.04	3
			duplicate	0.18	0.07	3
		100.6	1.3	0.23	0.02	2
			duplicate	0.25	0.12	3
		150.1	0.9	0.19	0.06	3
			duplicate	0.19	0.12	3

[a] SD is the standard deviation estimated from the double spike bracketing measurements of a single sample solution.
[b] n is the number of double spike bracketing measurements of a single sample solution.

Table 3
Dissolved barium (DBa) concentration and their stable barium isotopic composition ($\delta^{137}Ba_{DBa}$) data collected in various global rivers.

River	Location (°N, °E)	Sampling times	DBa (nmol kg^{-1})	$\delta^{137}Ba_{DBa}$ (‰)	2SD[a] (‰)	n[b]
Changjiang	31.8, 121.1	14 March 2015	432.0	0.06	0.06	3
		duplicate		−0.01	0.07	4
Amazon	0.0, −51.0	13 November 2013	143.7	0.04	0.11	3
Yukon	65.9, −149.7	27 August 2009	1466.6	0.06	0.07	2
Pearl	23.0, 113.5	01 August 2012	209.2	0.10	0.06	4
		duplicate		0.13	0.07	3
Sepik	−4.2, 143.8	08 June 2013	47.8	0.21	0.09	2
Danube	48.4, 10.0	31 August 2009	247.7	0.23	0.11	2
		duplicate		0.26	0.16	3
Lena	72.4, 126.7	20 August 2011	89.6	0.27	0.10	2
Colorado	N.A.[c]	06 November 2009	1048.8	0.29	0.08	3
		duplicate		0.31	0.10	3

[a] SD is the standard deviation estimated from the double spike bracketing measurements of a single sample solution.
[b] n is the number of double spike bracketing measurements of a single sample solution.
[c] N.A. denotes data not available.

2.2.1. Standard and double spike

Ba isotopic compositions are given in ‰ deviations relative to a Ba standard solution ($Ba(NO_3)_2$, Lot: C2-BA02050, Inorganic Ventures; $\delta^{137}Ba = [(^{137}Ba/^{134}Ba)_{sample}/(^{137}Ba/^{134}Ba)_{standard} - 1] \times 1000$). A ^{130}Ba–^{135}Ba double spike was prepared from $^{130}BaCO_3$ and $^{135}BaCO_3$ enriched by 35.8% and 93.4%, respectively (Oak Ridge National Laboratory). These were mixed gravimetrically to a ratio of 0.7/0.3 which is the ideal ratio calculated with the double spike toolbox by Rudge et al. (2009). Following the procedure adopted by Siebert et al. (2001), Ba isotopic ratios of both the standard and the spike were calibrated by doping a pure neodymium standard of known isotopic compositions (JNdi-1; Ali and Srinivasan, 2011) and mixtures of varying spike/standard ratios were then measured in pure Ba runs to test the accuracy of the calibration (Supplementary Fig. S1).

2.2.2. Chemical treatment and purification

The suspended particle samples were dissolved completely using the digestion method developed by Cardinal et al. (2001; reaction with concentrated acids (3 mL HCl + 2 mL HNO_3 + 1 mL HF) at 90 °C overnight). The lithogenic Ba content of <2% was deduced from aluminum (Al) concentrations in the digested solutions and indicates that these particles are almost exclusively of biogenic origin. The ^{130}Ba–^{135}Ba double spike was added to seawater and river water samples and solutions of digested suspended particle samples according to an ideal spike/sample ratio of 0.176 (Rudge et al., 2009) and allowed to equilibrate overnight. After drying down and redissolution in small amounts of 1 M HCl, Ba was separated from the sample matrix using cation-exchange chromatography. The application of a double spike accounts for any potential isotope fractionation during ion chromatographic separation but an average Ba yield of 90% was obtained for the entire chemical preparation procedure. By chemically treating 40 mL of Milli-Q water the same way as the seawater samples, the total procedural Ba blank was established to be <0.2 ng, which is <0.1% of the Ba introduced into the multicollector inductively coupled plasma mass spectrometry (MC-ICP-MS) for each sample solution (2 mL with a Ba concentration of ~100 ppb).

2.2.3. Mass spectrometry and data reduction

Ba isotopic compositions were determined in static mode on a Nu Plasma HR MC-ICP-MS at GEOMAR. Masses 128 (monitor of potential isobaric Xe interferences from impurities of the Ar plasma), 130, 132, 134, 135, 136 and 137 were measured simultaneously. A three-dimensional data reduction procedure following Siebert et al. (2001) was used, in which the exponential fractionation law was applied for both instrumental and natural mass-dependent fractionation (Miyazaki et al., 2014). Because the double spike method cannot correct for potential instrumental fractionation that does not follow the exponential fractionation law, each spiked sample measurement of $\delta^{137}Ba$ was "bracketed" and normalized to that of spiked Ba standard solution measurements (Siebert et al., 2001). External reproducibility is given as 2 standard deviation (2SD) of the average $\delta^{137}Ba$ value obtained from repeated measurements of the same sample solution during a single day, which varied between ±0.02 and ±0.17‰ (Tables 1–3) and represents the error bars of the field $\delta^{137}Ba$ data provided in this contribution (Figs. 2–5). The long-term external reproducibility for the replicate measurements of four standard reference materials and an in-house seawater matrix standard ranged between ±0.06 and ±0.10‰ (2SD) (Supplementary Fig. S2; Supplementary Table S1).

2.3. Si isotope analyses

The $\delta^{30}Si_{Si(OH)_4}$ values of the same seawater samples as those analyzed for stable Ba isotopic compositions have been published previously (Cao et al., 2012, 2015). Briefly, dissolved $Si(OH)_4$ was separated from the major matrix elements using a two-step brucite coprecipitation technique adapted from the MAGIC method (Karl and Tien, 1992). The precipitates were further purified using cation-exchange chromatography (Georg et al., 2006). Si isotopic compositions were determined in pseudo high-resolution mode on the Nu Plasma HR MC-ICP-MS. A standard–sample–standard bracketing technique was applied with a long-term external reproducibility of ±0.25‰ (2SD; Cao et al., 2015).

2.4. Analyses of other parameters

Detailed methods for analyzing concentrations of DBa and Ba_{xs} are provided in the Supplementary Material. Briefly, DBa concentrations in seawater were analyzed using an isotope dilution method (Klinkhammer and Chan, 1990; Freydier et al., 1995) on an Agilent 7500 quadrupole-ICP-MS with a reproducibility of ±2% (2SD). Ba_{xs} concentrations deposited on the filter membranes were calculated by the excess above lithogenic Ba/Al ratios (Jacquet et al., 2008). After a digestion in concentrated acids (Cardinal et al., 2001), both Ba and Al were also measured by the Agilent 7500 quadrupole-ICP-MS with precisions of ±2% (2SD).

$Si(OH)_4$, NO_3, and PO_4 concentration data were mainly obtained onboard using a Technicon AA3 Auto-Analyzer (Bran+Luebbe GmbH) following classical colorimetric methods. The precision for $Si(OH)_4$, NO_3, and PO_4 concentration measurements was within ±3%, ±1%, and ±2%, respectively (1SD; Du et al., 2013). In addition, NO_3 and PO_4 at nM levels in the surface mixed layer at station KK1 in the South China Sea were measured according to Zhang (2000) and Ma et al. (2008), respectively. Each method

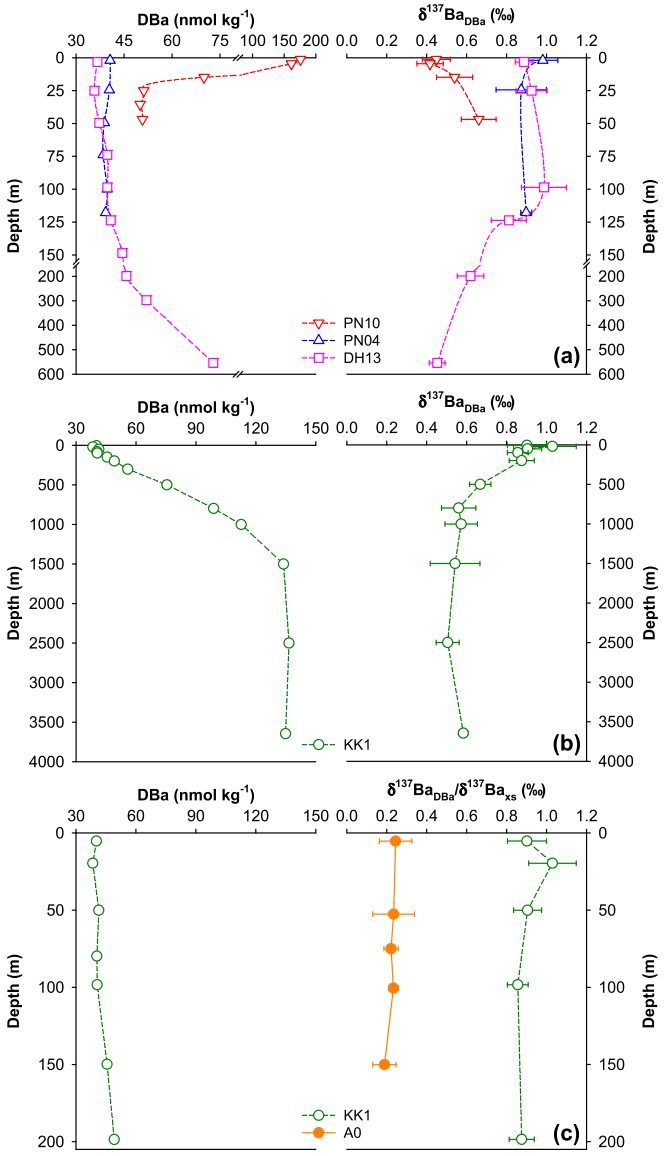

Fig. 2. Vertical distributions of dissolved barium (DBa) concentrations and their stable barium isotopic compositions ($\delta^{137}Ba_{DBa}$) in the East China Sea and the South China Sea. (a) Stations PN10, PN04, and DH13; (b) the entire water column at station KK1; (c) the upper 200 m at station KK1 (open circles) including the stable isotopic compositions of excess particulate barium ($\delta^{137}Ba_{Baxs}$) in the upper 150 m at station A0 (solid circles).

had a precision of better than ±5% (1SD). The nutrient concentration data collected at station KK1 have been published previously (Dai et al., 2013; Du et al., 2013). Vertical profiles of salinity and temperature were determined shipboard with a calibrated SBE-19-plus Conductivity–Temperature–Depth (CTD) recorder (Sea-Bird) attached to the Rosette sampler.

2.5. Steady state model describing Ba isotope fractionation

The steady state model assumes an open system with continuous supply of a given element with a specific isotopic composition (Sigman et al., 1999), which is demonstrated to be more realistic than a Rayleigh model (which assumes a closed system with no further supply from external sources; Mariotti et al., 1981) for Si isotope fractionation in the South China Sea and the East China Sea (Cao et al., 2012, 2015). The Ba isotope fractionation during removal of DBa within a steady state system is described by the following equations:

$$\delta^{137}Ba_{DBa\_1} = \delta^{137}Ba_{DBa\_0} - {}^{137}\varepsilon \times (1 - f) \quad (1)$$

$$\delta^{137}Ba_{Baxs\_1} = \delta^{137}Ba_{DBa\_0} - {}^{137}\varepsilon \times f = \delta^{137}Ba_{DBa\_1} + {}^{137}\varepsilon \quad (2)$$

$$f = \frac{[DBa]_1}{[DBa]_0} \quad (3)$$

The subscripts 1 and 0 denote evolved $\delta^{137}Ba_{DBa}$ or $\delta^{137}Ba_{Baxs}$ and DBa values at any given time and those prior to removal as the initial condition, respectively. ${}^{137}\varepsilon$ represents the fractionation factor of stable Ba isotopes between the particulate and dissolved phases. The term f reflects the fraction of remaining DBa relative to the initial concentration.

The apparent fractionation factor defined as $\Delta^{137}Ba$ (Eq. (4)) is the difference between the observed isotopic compositions of the Ba_{xs} product and the DBa substrate. Assuming that no Ba_{xs} accumulation occurs in the system, $\Delta^{137}Ba$ equals ${}^{137}\varepsilon$ in the steady state model.

$$\Delta^{137}Ba = \delta^{137}Ba_{Baxs\_1} - \delta^{137}Ba_{DBa\_1} \quad (4)$$

3. Results

3.1. $\delta^{137}Ba_{DBa}$ distributions in the East China Sea

A first important observation of this study is that all major rivers analyzed have relatively light $\delta^{137}Ba_{DBa}$ signatures ranging from 0.0 to +0.3‰ (Table 3). The surface waters at station PN10 on the East China Sea inner shelf, which are dominated by Changjiang Diluted Water (salinity below 28; Table 1; Cao et al., 2015), are enriched in DBa to up to 170 nmol kg^{-1} and have a surface $\delta^{137}Ba_{DBa}$ of +0.4‰ close to that of rivers thus clearly tracing the admixture of the river waters into seawater. $\delta^{137}Ba_{DBa}$ in the near-bottom waters at station PN10 is ~0.2‰ heavier than the river influenced surface waters and has more than three times lower DBa concentrations (Fig. 2a).

Further offshore in surface waters of station PN04 beyond the influence of Changjiang Diluted Water, DBa concentrations of 40 nmol kg^{-1} are markedly lower and the $\delta^{137}Ba_{DBa}$ signature close to +1.0‰ is significantly higher than at station PN10. Both DBa concentrations and $\delta^{137}Ba_{DBa}$ signatures are nearly constant throughout the water column (Fig. 2a) despite a surface mixed layer above 20 m at station PN04 (Supplementary Fig. S3; Cao et al., 2015).

Even further offshore at station DH13 on the East China Sea slope the surface water signatures down to 125 m depth are essentially identical in DBa concentrations (37–40 nmol kg^{-1}) and $\delta^{137}Ba_{DBa}$ signatures (+0.9‰) to station PN04. Below this depth DBa concentrations display a continuous increase to 73 nmol kg^{-1} near the bottom at 600 m water depth while $\delta^{137}Ba_{DBa}$ signatures show an overall inverse trend decreasing linearly to reach values of +0.5‰ in near-bottom waters (Fig. 2a).

3.2. $\delta^{137}Ba_{DBa}$ distributions at station KK1

At station KK1 in the open South China Sea basin, the vertical distributions of $\delta^{137}Ba_{DBa}$ also generally mirror those of DBa concentrations. DBa concentrations are essentially constant (~40 nmol kg^{-1}) in the upper 100 m. Below 150–200 m, DBa concentrations increase rapidly down to 1500 m water depth and remain stable at a value of 135 nmol kg^{-1} below (Figs. 2b and 2c). $\delta^{137}Ba_{DBa}$ values are constant within analytical uncertainty (+0.9‰) from the surface to 200 m depth and then decrease linearly to 800 m water depth. Below 800 m, $\delta^{137}Ba_{DBa}$ remain at

a stable value of +0.5‰ (Figs. 2b and 2c) suggesting homogenization by the strong vertical mixing in the interior of the South China Sea.

Note that both DBa concentrations and $\delta^{137}Ba_{DBa}$ signatures are essentially constant in the upper 100 m at values of ~40 nmol kg^{-1} and ~ +0.9‰ (Figs. 2a and 2c) despite a surface mixed layer above 25 and 60 m, respectively, at the open ocean stations DH13 and KK1 (Supplementary Fig. S3; Cao et al., 2015). Moreover, near-bottom waters around 600 m at station DH13 and those below 800 m at station KK1 have $\delta^{137}Ba_{DBa}$ values of +0.5‰. Given that the East China Sea and the South China Sea are two major marginal sea systems connected by offshore water mass exchange through the Kuroshio Current (Chen, 2008; Han et al., 2013), the consistent distribution of dissolved Ba isotopes likely reflects the control of inflowing Pacific Ocean waters.

4. Discussion

4.1. Nutrient-like fractionation

Distinct vertical $\delta^{137}Ba_{DBa}$ gradients of 0.4–0.5‰ are observed between the upper 100 m and the deep waters at station DH13 on the East China Sea slope and at station KK1 in the open South China Sea basin. The generally decreasing trend of $\delta^{137}Ba_{DBa}$ values with water depth is mirrored by increasing DBa concentrations (Figs. 2a and 2b), which is similar to those frequently found for dissolved Si isotope and concentration profiles (De La Rocha et al., 2000; Cao et al., 2012, 2015) supporting nutrient-like behavior of Ba in the ocean (Bacon and Edmond, 1972; Lea and Boyle, 1989; Jeandel et al., 1996; Jacquet et al., 2005; Roeske et al., 2012). The average $\delta^{137}Ba_{DBa}$ signature of all rivers analyzed is +0.16 ± 0.10‰ (1SD, $n = 8$; Table 3), which is significantly lower than that of +0.55 ± 0.05‰ of the average deep ocean (1SD, $n = 5$; below 800 m depth at station KK1; Table 1). This clearly demonstrates that Ba isotope fractionation with preferential removal of light Ba isotopes must occur in the upper ocean, where the primary DBa sources are riverine Ba inputs and regenerated Ba from deep waters (Dehairs et al., 1980). This is also strongly supported by our findings of relatively light $\delta^{137}Ba_{Baxs}$ signatures around +0.2‰ ($n = 5$) in biogenic particles in the upper 150 m at station A0 (Fig. 2c).

According to the global budget of Ba in the ocean suggested by Dehairs et al. (1980), riverine DBa inputs and regenerated DBa from deep waters to the upper ocean are 0.6 and 0.9 μg Ba cm^{-2} yr^{-1}, respectively, of which 90% of the total amount (i.e., 1.35 μg Ba cm^{-2} yr^{-1}) is removed by formation of particulate Ba. The DBa and their isotopic composition of the combined inputs from rivers and the deep ocean to the upper ocean are therefore 1.5 μg Ba cm^{-2} yr^{-1} (0.6 + 0.9) and +0.39 ± 0.07‰((0.6 × 0.16 + 0.9 × 0.55)/(0.6 + 0.9)). Following a steady state model (Eqs. (1) and (3)) and assuming a fractionation factor ($^{137}\varepsilon$) of −0.7‰ (i.e., Δ^{137}Ba as the difference between average $\delta^{137}Ba_{Baxs}$ (+0.2‰) and $\delta^{137}Ba_{DBa}$ (+0.9‰) observed in the upper 150 m beyond the river influence in this study; Eq. (4)), removal of 1.35 μg Ba cm^{-2} yr^{-1} indeed results in a $\delta^{137}Ba_{DBa}$ value of +1.02 ± 0.07‰, which is consistent with our field observations in the upper water column (Table 1). This good first order agreement implies that from a perspective of isotope mass balance, other sources of Ba in the upper ocean, such as hydrothermal activity, submarine groundwater discharge and atmospheric inputs are not important or their signatures cancel each other out. Given that our first order mass balance is mainly based on regional observations and an early budget (Dehairs et al., 1980), further global scale constraints on the isotopic composition of major Ba reservoirs are needed for a comprehensive budgeting of Ba in the ocean.

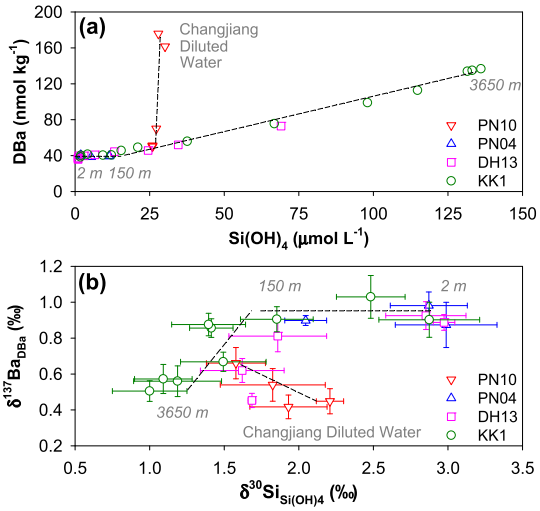

Fig. 3. (a) DBa versus Si(OH)$_4$ and (b) $\delta^{137}Ba_{DBa}$ versus $\delta^{30}Si_{Si(OH)_4}$ for samples collected in the East China Sea and the South China Sea. The dashed lines in each panel indicate trends of the DBa–Si(OH)$_4$ and the $\delta^{137}Ba_{DBa}$–$\delta^{30}Si_{Si(OH)_4}$ relationships. The numbers in italics denote the sampling depth of the endpoints of each line excluding station PN04 influenced by the Changjiang Diluted Water. Si(OH)$_4$ and $\delta^{30}Si_{Si(OH)_4}$ data collected in the East China Sea are from Cao et al. (2015). $\delta^{137}Ba_{DBa}$ at station KK1 was compared to $\delta^{30}Si_{Si(OH)4}$ at station SEATS (18.0°N, 116.0°E) occupied during the same cruise to the South China Sea (Cao et al., 2012) and located ~50 km southeast of station KK1.

4.2. Comparison with Si isotope distributions

It is likely that either direct uptake by plankton or adsorption onto biogenic particles (Ganeshram et al., 2003) causes fractionation towards lighter particulate Ba isotopes and correspondingly heavier dissolved $\delta^{137}Ba_{DBa}$ in the uppermost water column of the ocean. We constrain the biological effects on Ba isotopic compositions by comparing with Si, which is a major nutrient in the ocean controlling the diatom life cycle. DBa distributions broadly resemble those of Si(OH)$_4$ in that both display a surface enrichment at the nearshore station PN10 and a general increase from the surface to the near-bottom at the offshore stations DH13 and KK1 (Figs. 2a and 2b; Supplementary Fig. S4; Cao et al., 2015). A more detailed comparison of the DBa and Si(OH)$_4$ concentrations (Fig. 3a), however, reveals significant differences. At station PN10, in contrast to relatively constant Si(OH)$_4$ concentrations, the surface DBa concentrations show a large increase originating from the river discharge highly enriched in Ba, analogous to previous observations in other river-dominated areas of the ocean (e.g., Guay and Falkner, 1998). The apparently lower degree of Si(OH)$_4$ enrichment in Changjiang Diluted Water probably results from biological consumption of Si along the river (Si(OH)$_4$ ~100 μmol L^{-1}; Li et al., 2007) to the mouth of the Changjiang river estuary (Si(OH)$_4$ ~30 μmol L^{-1}; Cao et al., 2015), where diatoms are dominant in summer (Furuya et al., 2003; Guo et al., 2014). At the other three stations, the comparison displays two general trends. In the upper 150 m, DBa concentrations are almost constant whereas those of Si(OH)$_4$ sharply increase from depleted values near 0 μmol L^{-1} in the surface mixed layer to about 15 μmol L^{-1} in the subsurface waters. Below 150 m depth, DBa and Si(OH)$_4$ display a positive linear relationship (Fig. 3a). Note that this covariance, mainly resulting from similar sites of removal and regeneration, is a consequence of ocean circulation (Lea and Boyle, 1989).

Comparing the isotopic compositions it is clear that both $\delta^{137}Ba_{DBa}$ and $\delta^{30}Si_{Si(OH)_4}$ values in Changjiang Diluted Water are markedly lower than those in the offshore surface waters due to riverine inputs with overall light isotopic compositions. Similar to the vertical distribution of $\delta^{30}Si_{Si(OH)_4}$, $\delta^{137}Ba_{DBa}$ at stations DH13 and KK1 generally decreases with depth mirrored by an increase

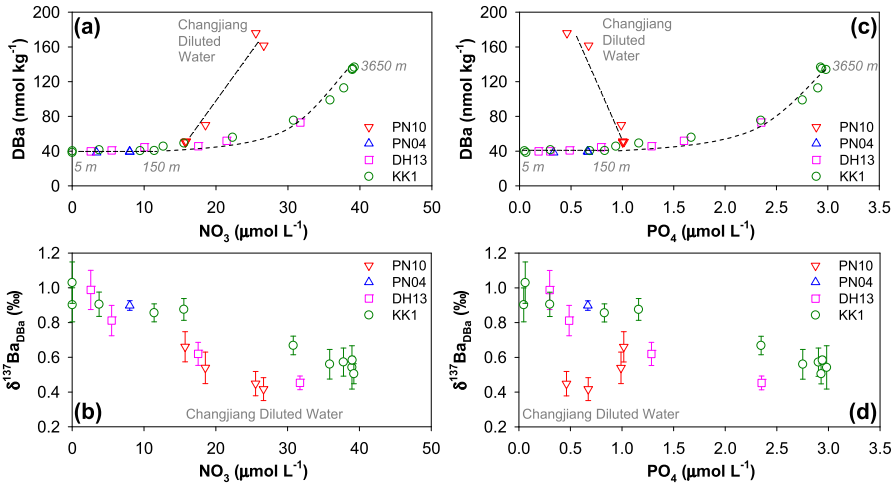

Fig. 4. Ba versus NO_3 and PO_4 for samples collected in the East China Sea and the South China Sea. (a) DBa versus NO_3; (b) $\delta^{137}Ba_{DBa}$ versus NO_3; (c) DBa versus PO_4; (d) $\delta^{137}Ba_{DBa}$ versus PO_4. The dashed lines in (a) and (c) indicate trends of the DBa–NO_3 and the DBa–PO_4 relationships. The numbers in italics in (a) and (c) denote the sampling depth of the endpoints of each line excluding station PN04 influenced by the Changjiang Diluted Water. Note that concentrations of NO_3 and PO_4 in the upper 50–75 m at stations PN04 and DH13 were too low to be determined using classical colorimetric methods, while those in the surface mixed layer at station KK1 were measured by techniques targeting low-concentration nutrients at nM levels (Zhang, 2000; Ma et al., 2008). NO_3 and PO_4 data collected at station KK1 in the South China Sea are from Dai et al. (2013) and Du et al. (2013).

in the concentrations (Figs. 2a and 2b; Cao et al., 2012, 2015). Nevertheless, significant differences exist between the isotopic compositions of the two elements as documented by three distinct trends in the $\delta^{137}Ba_{DBa}$–$\delta^{30}Si_{Si(OH)_4}$ plot (Fig. 3b). At station PN10, due to mixing of the Changjiang Diluted Water with low $\delta^{137}Ba_{DBa}$ and high $\delta^{30}Si_{Si(OH)_4}$ (probably enhanced by biological fractionation during diatom growth) relative to the corresponding near-bottom waters, a negative relationship is observed between the two parameters. In the upper 150 m at the other three stations, $\delta^{137}Ba_{DBa}$ signatures are nearly constant as opposed to the rapid ~1.0‰ decrease of $\delta^{30}Si_{Si(OH)_4}$ from the surface to the subsurface waters. Although dissolved Ba and Si isotopes are not as well correlated as their concentrations below 150 m, a generally positive relationship documents that both systems become lighter in the intermediate and deep waters with increasing depth, most likely as a consequence of water mass mixing (Fig. 3b).

The decoupling between $\delta^{137}Ba_{DBa}$ and $\delta^{30}Si_{Si(OH)_4}$, in the river plume and in the upper ocean, confirms that there is no direct association of Ba and diatom growth and that Ba is a much less bioactive element compared to Si, which is often biolimiting in the marine environment (Guay and Falkner, 1997). This is consistent with observations in culture experiments showing very low cellular Ba concentrations in diatoms (Fisher et al., 1991; Sternberg et al., 2005).

In order to constrain the role of overall surface ocean productivity in fractionating Ba isotopes we compare our Ba results with concentrations of NO_3 and PO_4, the two other major nutrients in the ocean, which are essential for all phytoplankton. Beyond the influence of Changjiang Diluted Water, DBa concentrations and $\delta^{137}Ba_{DBa}$ signatures in the upper 150 m are essentially constant whereas concentrations of both NO_3 and PO_4 rapidly increase from the very surface waters to the subsurface (Fig. 4) implying overall minor effects of surface biology on Ba dynamics. Such decoupling between DBa and NO_3 or PO_4 extends to the subsurface and deep waters below 150 m (Figs. 4a and 4c), which is also observed for other oceanic regimes (e.g., Horner et al., 2015). Given that active intracellular uptake by living phytoplankton rarely occurs, surface DBa, in contrast to the major nutrients, is not as strongly depleted and is thus not reflected by significantly heavier $\delta^{137}Ba_{DBa}$ signatures in the very surface waters. While negligible biological utilization does not induce apparent gradients of DBa and $\delta^{137}Ba_{DBa}$ in the upper 100 m, there is also no trend with salinity, which documents a pronounced stratification in the upper 20–60 m (Supplementary Fig. S3). We contend that passive adsorption onto particles of mainly biogenic origin combined with DBa supply from deep waters via vertical mixing can best explain its observed distribution in the uppermost water column. During this process, the preferential removal of the lighter isotopes induces higher $\delta^{137}Ba_{DBa}$ and lower $\delta^{137}Ba_{Baxs}$ and both signatures are also essentially constant.

4.3. Tracing water mass mixing

Given that direct biological uptake is obviously quantitatively unimportant at our study sites, the significant spatial variations of $\delta^{137}Ba_{DBa}$ are primarily a consequence of physical mixing between different water masses. In the East China Sea, three major water mass end-members (i.e., Changjiang Diluted Water, East China Sea (sub)surface water, and East China Sea deep water) with distinct DBa concentrations and isotopic compositions can be distinguished in a $\delta^{137}Ba_{DBa}$–1/DBa plot (Fig. 5a). Although $\delta^{137}Ba_{DBa}$ values of Changjiang Diluted Water and East China Sea deep water are within analytical uncertainty identical, the former is markedly enriched in DBa. $\delta^{137}Ba_{DBa}$ signatures are significantly heavier in the East China Sea (sub)surface water where much lower DBa concentrations prevail. All other data points can be fully explained by two separate two-end-member mixing lines constrained by the three major water masses (Fig. 5a).

In the South China Sea, all data points collected at station KK1 follow a strict linear relationship between $\delta^{137}Ba_{DBa}$ and 1/DBa ($r^2 = 0.95$; Fig. 5b), which suggests that a simple two-end-member mixing of the highly fractionated South China Sea (sub)surface water and the South China Sea deep water with low $\delta^{137}Ba_{DBa}$ can explain the $\delta^{137}Ba_{DBa}$ distributions. Potential effects of other processes affecting the Ba isotopic compositions (e.g., horizontal mixing from the nearby slope area, production/dissolution of Ba_{xs} or barite) are at this point probably too small to be detected outside analytical uncertainty of the $\delta^{137}Ba_{DBa}$ signatures and thus cannot be distinguished from the dominant control of water mass mixing.

5. Conclusions

Our analyses of the distribution of $\delta^{137}Ba_{DBa}$ in different oceanic regimes in the East China Sea and the South China Sea

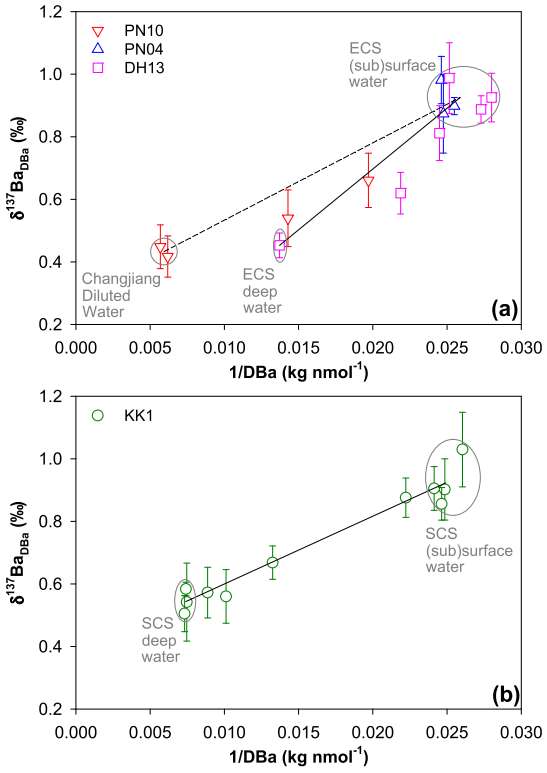

Fig. 5. $\delta^{137}Ba_{DBa}$ versus 1/DBa for samples collected in (a) the East China Sea (ECS) and (b) the South China Sea (SCS). In (a), the dashed line indicates the horizontal mixing between the Changjiang Diluted Water and the ECS surface water, while the solid line indicates the vertical mixing between the ECS (sub)surface water and the ECS deep water; In (b), the solid line indicates the vertical mixing between the SCS (sub)surface water and the SCS deep water.

reveal significant spatial variations primarily owing to physical mixing between various water masses and to some extent biological effects. The dynamics of dissolved Ba isotopes are broadly similar to those of dissolved Si isotopes but there is also clear decoupling between these isotope systems in the upper water column. Combined with the decoupling of DBa and $\delta^{137}Ba_{DBa}$ from NO_3 or PO_4 concentrations, we contend that Ba is not directly physiologically utilized and in particular is not associated with silica frustules of diatoms.

The results suggest that Ba isotopes are a new useful tracer of land–sea interactions and water mass mixing, in particular of the advection of river waters with distinctly elevated DBa concentrations and light isotopic compositions. Similar to Ba/Ca ratios of surface-dwelling planktonic foraminifera (e.g., Weldeab et al., 2007), the $\delta^{137}Ba$ of carbonates may also prove a quantitative proxy for paleosalinity in proximity to large river plumes. On the other hand, the largest vertical gradient of $\delta^{137}Ba_{DBa}$ is observed in the intermediate waters where the majority of the mesopelagic barite forms. If this process contributes significantly to the water mass isotope signatures in comparison to physical mixing, Ba isotopic compositions of barites may be a potential proxy for paleoproductivity or nutrient utilization. This needs to be tested through systematic analyses of particulate Ba isotopic compositions in both the water column and the sediments.

Acknowledgements

Zhimian Cao was supported by a Research Fellowship for postdoctoral researchers by the Alexander von Humboldt Foundation. This work was funded by the National Key Scientific Research Project (2015CB954000) sponsored by the Ministry of Science and Technology of the People's Republic of China. We thank Volker Liebetrau, Weidong Zhai, Zhouling Zhang, Georgi Laukert, and Gila Merschel for providing the river water samples and Jianyu Hu for providing the CTD data. Feifei Meng, Kai Wu, Chuanjun Du, Lifang Wang, Yanping Xu, Tao Huang, and the crew of R/V *Dongfanghong II* are thanked for their assistance in sampling and/or analysis. We are also grateful to the inspiring comments from Shuh-Ji Kao. Constructive comments by Thomas Nägler and two anonymous reviewers significantly improved the quality of this contribution.

Appendix A. Supplementary material

Supplementary material related to this article can be found online at http://dx.doi.org/10.1016/j.epsl.2015.11.017.

References

Ali, A., Srinivasan, G., 2011. Precise thermal ionization mass spectrometric measurements of $^{142}Nd/^{144}Nd$ and $^{143}Nd/^{144}Nd$ isotopic ratios of Nd separated from geological standards by chromatographic methods. Int. J. Mass Spectrom. 299, 27–34.

Bacon, M.P., Edmond, J.M., 1972. Barium at GEOSECS III in the Southwest Pacific. Earth Planet. Sci. Lett. 16, 66–74.

Böttcher, M.E., Geprägs, P., Neubert, N., von Allmen, K., Pretet, C., Samankassou, E., Nägler, T.F., 2012. Barium isotope fractionation during experimental formation of the double carbonate $BaMn[CO_3]_2$ at ambient temperature. Isot. Environ. Healt, 1–7. http://dx.doi.org/10.1080/10256016.2012.673489.

Cao, Z., Dai, M., 2011. Shallow-depth $CaCO_3$ dissolution: evidence from excess calcium in the South China Sea and its export to the Pacific Ocean. Glob. Biogeochem. Cycles 25, GB2019. http://dx.doi.org/10.1029/2009GB003690.

Cao, Z., Frank, M., Dai, M., Grasse, P., Ehlert, C., 2012. Silicon isotope constraints on sources and utilization of silicic acid in the northern South China Sea. Geochim. Cosmochim. Acta 97, 88–104.

Cao, Z., Frank, M., Dai, M., 2015. Dissolved silicon isotopic compositions in the East China Sea: water mass mixing vs. biological fractionation. Limnol. Oceanogr. 60, 1619–1633. http://dx.doi.org/10.1002/lno.10124.

Cardinal, D., Dehairs, F., Cattaldo, T., André, L., 2001. Geochemistry of suspended particles in the Subantarctic and Polar Front Zones south of Australia: constraints of export and advection processes. J. Geophys. Res. 106, 31637–31656.

Chen, C.-T.A., 2008. Distributions of nutrients in the East China Sea and the South China Sea Connection. J. Oceanogr. 64, 737–751.

Dai, M., Cao, Z., Guo, X., Zhai, W., Liu, Z., Yin, Z., Xu, Y., Gan, J., Hu, J., Du, C., 2013. Why are some marginal seas sources of atmospheric CO_2? Geophys. Res. Lett. 40, 2154–2158. http://dx.doi.org/10.1002/grl.50390.

Dehairs, F., Chesselet, R., Jedwab, J., 1980. Discrete suspended particles of barite and the barium cycle in the open Ocean. Earth Planet. Sci. Lett. 49, 528–550.

Dehairs, F., Shopova, D., Ober, S., Veth, C., Goeyens, L., 1997. Particulate barium stocks and oxygen consumption in the Southern Ocean mesopelagic water column during spring and early summer: relationship with export production. Deep-Sea Res. II 44, 497–516.

De La Rocha, C.L., Brzezinski, M.A., DeNiro, M.J., 2000. A first look at the distribution of the stable isotopes of silicon in natural water. Geochim. Cosmochim. Acta 64, 2467–2477.

Du, C., Liu, Z., Dai, M., Kao, S.-J., Cao, Z., Zhang, Y., Huang, T., Wang, L., Li, Y., 2013. Impact of the Kuroshio intrusion on the nutrient inventory in the upper northern South China Sea: insights from an isopycnal mixing model. Biogeosciences 10, 6419–6432.

Fisher, N.S., Guillard, R.R.L., Bankston, D.C., 1991. The accumulation of barium by marine phytoplankton grown in culture. J. Mar. Res. 49, 339–354.

Freydier, R., Dupre, B., Polve, M., 1995. Analyses by inductively coupled plasma mass spectrometry of Ba concentrations in water and rock samples. Comparison between isotope dilution and external calibration with or without internal standard. Eur. Mass Spectrom. 1, 283–291.

Furuya, K., Hayashi, M., Yabushita, Y., Ishikawa, A., 2003. Phytoplankton dynamics in the East China Sea in spring and summer as revealed by HPLC-derived pigment signatures. Deep-Sea Res. II 50, 367–387.

Ganeshram, R.S., François, R., Commeau, J., Brown-Leger, S.L., 2003. An experimental investigation of barite formation in seawater. Geochim. Cosmochim. Acta 67, 2599–2605.

Georg, R.B., Reynolds, B.C., Frank, M., Halliday, A.N., 2006. New sample preparation techniques for the determination of Si isotopic compositions using MC-ICPMS. Chem. Geol. 235, 95–104.

Guay, C.K., Falkner, K.K., 1997. Barium as a tracer of Arctic halocline and river waters. Deep-Sea Res. II 44, 1543–1569.

Guay, C.K., Falkner, K.K., 1998. A survey of dissolved barium in the estuaries of major Arctic rivers and adjacent seas. Cont. Shelf Res. 18, 859–882.

Guo, S., Feng, Y., Wang, L., Dai, M., Liu, Z., Bai, Y., Sun, J., 2014. Seasonal variation in the phytoplankton community of a continental-shelf sea: the East China Sea. Mar. Ecol. Prog. Ser. 516, 103–126. http://dx.doi.org/10.3354/meps10952.

Han, A., Dai, M., Gan, J., Kao, S.-J., Zhao, X., Jan, S., Li, Q., Lin, H., Chen, C.-T.A., Wang, L., Hu, J., Wang, L., Gong, F., 2013. Inter-shelf nutrient transport from the East China Sea as a major nutrient source supporting winter primary production on the northeast South China Sea shelf. Biogeosciences 10, 8159–8170.

Horner, T.J., Kinsley, C.W., Nielsen, S.G., 2015. Barium-isotopic fractionation in seawater mediated by barite cycling and ocean circulation. Earth Planet. Sci. Lett. 430, 511–522.

Immenhauser, A., Buhl, D., Richter, D., Niedermayr, A., Riechelmann, D., Dietzel, M., Schulte, U., 2010. Magnesium-isotope fractionation during low-Mg calcite precipitation in a limestone cave – field study and experiments. Geochim. Cosmochim. Acta 74, 4346–4364.

Jacquet, S.H.M., Dehairs, F., Cardinal, D., Navez, J., Delille, B., 2005. Barium distribution across the Southern Ocean frontal system in the Crozet-Kerguelen Basin. Mar. Chem. 95, 149–162.

Jacquet, S.H.M., Savoye, N., Dehairs, F., Strass, V.H., Cardinal, D., 2008. Mesopelagic carbon remineralization during the European Iron Fertilization Experiment. Glob. Biogeochem. Cycles 22, GB1023. http://dx.doi.org/10.1029/2006GB002902.

Jeandel, C., Dupré, B., Lebaron, G., Monnin, C., Minster, J.-F., 1996. Longitudinal distributions of dissolved barium, silica and alkalinity in the western and southern Indian Ocean. Deep-Sea Res. I 43, 1–31.

Karl, D.M., Tien, G., 1992. MAGIC: a sensitive and precise method for measuring dissolved phosphorus in aquatic environments. Limnol. Oceanogr. 37, 105–116.

Klinkhammer, G.P., Chan, L.H., 1990. Determination of barium in marine waters by isotope dilution inductively coupled plasma mass spectrometry. Anal. Chim. Acta 232, 323–329.

Lea, D., Boyle, E., 1989. Barium content of benthic foraminifera controlled by bottom-water composition. Nature 338, 751–753.

Li, M., Xu, K., Watanabe, M., Chen, Z., 2007. Long-term variations in dissolved silicate, nitrogen, and phosphorus flux from the Yangtze River into the East China Sea and impacts on estuarine ecosystem. Estuar. Coast. Shelf Sci. 71, 3–12.

Ma, J., Yuan, D., Liang, Y., 2008. Sequential injection analysis of nanomolar soluble reactive phosphorus in seawater with HLB solid phase extraction. Mar. Chem. 111, 151–159.

Mariotti, A., Germon, J.C., Hubert, P., Kaiser, P., Letolle, R., Tardieux, A., Tardieux, P., 1981. Experimental determination of nitrogen kinetic isotope fractionation: some principles; Illustration for the denitrification and nitrification processes. Plant Soil 62, 413–430.

McManus, J., Berelson, W.M., Klinkhammer, G.P., Johnson, K.S., Coale, K.H., Anderson, R.F., Kumar, N., Burdige, D.J., Hammond, D.E., Brumsack, H.J., McCorkle, D.C., Rushdi, A., 1998. Geochemistry of barium in marine sediments: implications for its use as a paleoproxy. Geochim. Cosmochim. Acta 62, 3453–3473.

Miyazaki, T., Kimura, J.-I., Chang, Q., 2014. Analysis of stable isotope ratios of Ba by double-spike standard–sample bracketing using multiple-collector inductively coupled plasma mass spectrometry. J. Anal. At. Spectrom. 29, 483–490.

Nan, X., Wu, F., Zhang, Z., Hou, Z., Huang, F., Yu, H., 2015. High-precision barium isotope measurement by MC-ICP-MS. J. Anal. At. Spectrom. 30, 2307–2315.

Nürnberg, C.C., Bohrmann, G., Schlüter, M., Frank, M., 1997. Barium accumulation in the Atlantic sector of the Southern Ocean: results from 190,000-year records. Paleoceanography 12, 594–603.

Paytan, A., Griffith, E.M., 2007. Marine barite: recorder of variations in ocean export productivity. Deep-Sea Res. II 54, 687–705.

Paytan, A., Kastner, M., Chavez, F.P., 1996. Glacial to interglacial fluctuations in productivity in the Equatorial Pacific as indicated by marine barite. Science 274, 1355–1357.

Roeske, T., Rutgers vd Loeff, M., Middag, R., Bakker, K., 2012. Deep water circulation and composition in the Arctic Ocean by dissolved barium, aluminium and silicate. Mar. Chem. 132–133, 56–67.

Rudge, J.F., Reynolds, B.C., Bourdon, B., 2009. The double spike toolbox. Chem. Geol. 265, 420–431.

Schlitzer, R., 2015. Ocean data view 4. http://odv.awi.de.

Siebert, C., Nägler, T.F., Kramers, J.D., 2001. Determination of molybdenum isotope fractionation by double-spike multicollector inductively coupled plasma mass spectrometry. Geochem. Geophys. Geosyst. 2, 1032. http://dx.doi.org/10.1029/2000GC000124.

Sigman, D.M., Altabet, M.A., McCorkle, D.C., Francois, R., Fischer, G., 1999. The δ^{15}N of nitrate in the Southern Ocean: consumption of nitrate in surface waters. Glob. Biogeochem. Cycles 13, 1149–1166.

Sternberg, E., Tang, D., Ho, T.-Y., Jeandel, C., Morel, F.M.M., 2005. Barium uptake and adsorption in diatoms. Geochim. Cosmochim. Acta 69, 2745–2752.

von Allmen, K., Böttcher, M.E., Samankassou, E., Nägler, T.F., 2010. Barium isotope fractionation in the global barium cycle: first evidence from barium minerals and precipitation experiments. Chem. Geol. 277, 70–77.

Weldeab, S., Lea, D.W., Schneider, R.R., Andersen, N., 2007. 155,000 years of West African monsoon and ocean thermal evolution. Science 316, 1303–1307.

Zhai, W., Dai, M., 2009. On the seasonal variation of air–sea CO_2 fluxes in the outer Changjiang (Yangtze River) Estuary, East China Sea. Mar. Chem. 117, 2–10.

Zhang, J.-Z., 2000. Shipboard automated determination of trace concentrations of nitrite and nitrate in oligotrophic water by gas-segmented continuous flow analysis with a liquid wave guide capillary flow cell. Deep-Sea Res. I 47, 1157–1171.